Universal features of the stick-slip dynamics of an intruder moving through a confined granular medium

Luis A. Pugnaloni, C. Manuel Carlevaro, Ryan Kozlowski, Hu Zheng, Lou Kondic, and Joshua E. S. Socolar

Universal features of the stick–slip dynamics of an intruder moving through a confined granular medium

Luis A. Pugnaloni,[1,][*] C. Manuel Carlevaro,[2] Ryan Kozlowski,[3] Hu Zheng,[4] Lou Kondic,[5] and Joshua E. S. Socolar[6]

[1]*Departamento de Física, Facultad de Ciencias Exactas y Naturales,*
Universidad Nacional de La Pampa, CONICET,
Uruguay 151, 6300 Santa Rosa (La Pampa), Argentina
[2]*Instituto de Física de Líquidos y Sistemas Biológicos, CONICET, 59 789, 1900 La Plata, Argentina*
and Departamento de Ingeniería Mecánica, Universidad Tecnológica Nacional,
Facultad Regional La Plata, Av. 60 Esquina 124, La Plata, 1900, Argentina
[3]*Physics Department, Berea College, Berea, Kentucky 40404, USA*
[4]*Department of Geotechnical Engineering, College of Civil Engineering, Tongji University, Shanghai, 200092, China*
[5]*Department of Mathematical Sciences and Center for Applied Mathematics and Statistics,*
New Jersey Institute of Technology, Newark, New Jersey 07102, USA
[6]*Department of Physics, Duke University, Durham, North Carolina 27708, USA*

Experiments and simulations of an intruder dragged by a spring through a 2D annulus of granular material exhibit robust force fluctuations. At low packing fractions ($\phi < \phi_0$), the intruder clears an open channel. Above ϕ_0, stick–slip dynamics develop, with an average energy release that is independent of the particle-particle and particle-base friction coefficients but does depend on the width W of the annulus and the diameter D of the intruder. A simple model predicts the dependence of ϕ_0 on W and D, allowing for a data collapse for the average energy release as a function of ϕ/ϕ_0. These results pose challenges for theories of mechanical failure in amorphous materials.

The reaction force associated with the deformation of a sample subjected to an intruding object is a fundamental characteristic of the material. For granular materials such as soils, penetration tests using intruders that are large compato the grain size are routine techniques to evaluate their mechanical properties [1]. Interest in the micro-mechanics of granular materials has also prompted studies of the response of photoelastic granular materials to loads applied at the grain scale [2–6]. In recent decades there has been interest in the dynamical response of granular materials to intruding objects that are dragged through the bulk of the sample [7–13]. In most cases the intruders are much larger than the grains that form the relevant part of the material, but there is also growing interest in the response to a grain-sized intruder, as such a setup provides insight into the micro-mechanics of granular media rather than bulk properties [14].

In this letter we report results from experiments and simulations on the stick–slip dynamics of a grain-size intruder driven through a circular annulus with fixed boundaries filled with photoelastic disks. We find that the energy dissipation associated with slip events is insensitive to the details of the particle–particle interactions and depends in a surprisingly simple manner on the packing fraction ϕ, the system size W, and the intruder size D. The granular sample is confined at constant volume and we drive the intruder in the azimuthal direction at a fixed radius. We find a critical packing fraction ϕ_0 (which increases for increasing width W and decreasing intruder size D) below which the intruder clears an open channel in the material and moves freely after a few revolutions. Moreover, we show that data for the average amount of

energy dissipated in a slip event collapses when plotted against the rescaled parameter $\phi/\phi_0 - 1$. Using a simple model, we predict that $\phi_0 = \phi_{\max}(W - D - 2kd)/W$, where d is the typical grain size, $\phi_{\max}$ is the maximum bulk packing fraction, and k is a phenomenological $O(1)$ parameter that characterizes the width of the lower density boundary layers bordering the open channel. We note that the dependence on W suggests that in this system the stick-slip dynamics is a finite-size effect. As W increases, the range of packing fractions supporting stick-slip dynamics shrinks, presumably approaching zero in the infinite system limit.

The system – The considegranular system is composed of a bidisperse mixture of disks forming a quasi-two-dimensional (2D) monolayer through which an intruding particle is pulled (see sketch in Fig. 1). The diameter ratio between small (d_s) and large (d_l) disks is $\approx d_l/d_s \approx 1.25$ and the number ratio of small to large disks approximately 1.1:1. (A 2.75:1 ratio was also tested for a few sets). We note that the response of a granular sample is strongly dependent on the boundary conditions imposed (constant pressure versus constant volume) and the forcing protocol (constant force versus constant velocity) [14, 16–19]. In the present case, the medium is confined to a fixed-volume annular area of inner radius R_{in}, radial width W, and outer radius $R_{in} + W$. The intruding particle, with diameter D, is pushed by a torque spring at a fixed radius $R_{in} + W/2$. The end of the spring not attached to the intruder is rotated at a low, fixed rate to slowly apply stress on the granular medium via the localized intruding grain. At high packing fractions stick–slip dynamics are observed. When in the stick-slip regime, the medium exhibits *sticking periods* of quasi-
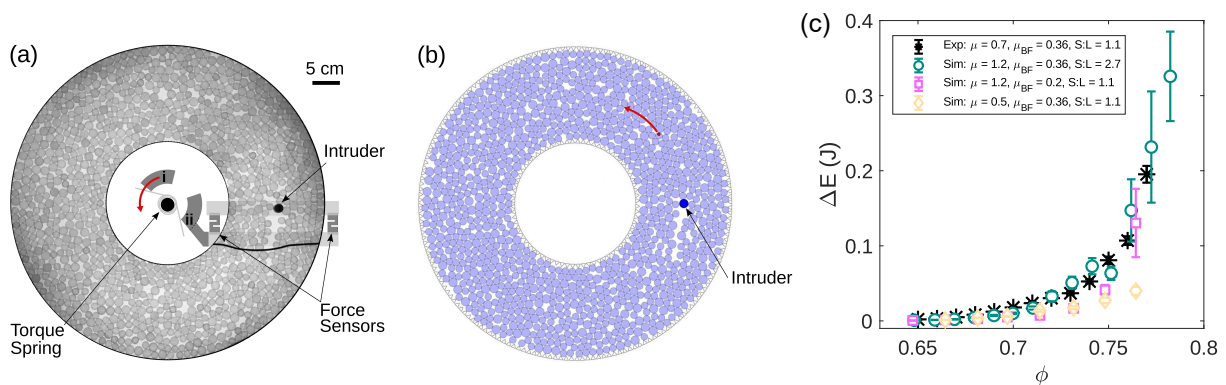
FIG. 1. (a) Schematic of the experimental setup. The end (i) of the torque spring is driven at a constant angular velocity while the end (ii) is fixed to the arm that holds the intruder. The 2D granular medium is composed of a layer of bidisperse polyurethane disks. (b) Sample snapshot of a simulation. The dot indicates the driven end of the torque spring. The other end of the spring is attached to the intruder (dark blue particle). The static inner and outer boundaries are formed by equilateral triangles. Reproduced with permission from Ref. [15]. (c) Mean energy drop at the slips $\langle \Delta E \rangle$ as a function of ϕ for different mix ratios, basal friction coefficients and particle–particle friction coefficients (experiments and simulations). Error bars correspond to the standard error of the mean. As a reference, the elastic energy of the torque spring when compressed by the angle subtended by 10 small particle radii at the radial position of the intruder is 0.09 J.

static particle configurations and increasing stress interspersed with rapid stress-relieving *slip events* in which the medium plastically deforms and the intruder slides in the azimuthal direction until a stable configuration of grains stops it, initiating a new sticking periods. In all cases, the driving rate is sufficiently slow that decreasing it further causes no observable change in the stick-slip dynamics.

As the intruder penetrates the system, significant heterogeneities form in the local packing fraction. Most importantly, the intruder leaves an open area (wake) behind it as grains are densely packed into the annular areas outside of the intruder's path. As the global packing fraction decreases, the extent of the wake behind the intruder grows on average until, at a low enough *global* packing fraction, it becomes an open channel that extends all the way around the annulus so that the intruder no longer interacts with any grains. To understand the dynamics of the intruder as the channel length approaches the entire length of the intruder's path, we vary ϕ and D (both in experiments and simulations) and W (in simulations only). Details of the experiments and simulation methods can be found in previous papers [15, 20]. Here we provide only a brief description.

In experiments, the intruding particle is suspended from a cantilever into the quasi-two-dimensional annular channel of disks. A stepper motor rotates one end of a torque spring (stiffness $\kappa_0 = 0.38$ Nm/rad) at a fixed rate ($\omega_0 = 0.12$ rad/s) and the cantilever is attached to the other end of the spring. The bidisperse polyurethane disks have interparticle friction $\mu = 0.7 \pm 0.1$ and basal friction $\mu_{BF} = 0.25 \pm 0.05$, and are of sizes $d_s = 1.280 \pm 0.001$ cm and $d_l = 1.601 \pm 0.002$ cm. The inner radius of the channel is $R_{in} \approx 8.4 d_s$, and the width

is $W \approx 14 d_s$. Load cells measure the total force that the grains exert on the intruder, and the dynamics of the intruder is monitored via video tracking. Experiments are done with various packing fractions for each of six intruder sizes $D = [5.2, 3.7, 3.0, 2.0, 1.5, 1.0]d_s$.

In simulations, we model this system using Box2D, a contact dynamics discrete element approach developed for handling perfectly rigid bodies of arbitrary shape [21]. The parameters in this system, such as friction coefficients and size ratios, are consistent with those of the experiments; excellent agreement has been found between experiments and simulations of this system in previous work [15]. In the simulations, ϕ, basal friction, intergrain friction, small to large grain ratio, pulling spring constant, D, and W are varied.

Results – To characterize the stick–slip steady state dynamics, we have measured the drop, ΔE, of the spring potential energy at each slip event, determining its mean and standard error. A sample time series of the force sensor, distributions of ΔE showing that its mean value is a meaningful statistical descriptor, and data for additional measures such as force drop and duration of sticking periods, are presented in the Supplementary Material [22].

Figure 1(c) shows the average, $\langle \Delta E \rangle$, over the set of detected slip events as a function of ϕ for a set of experiments and simulations with $D = 1.26 d_s$ and different small to large grain ratios, particle-base friction coefficients, and interparticle friction coefficients. Below $\phi_0 \approx 0.64$ the stick–slip dynamics is no longer observed due to the formation, after a few revolutions of the intruder, of an open channel in the granular medium that allows the intruder to move without contacting any particles. When ϕ approaches the jamming value of ≈ 0.8, there is an apparent divergence in the mean energy drop
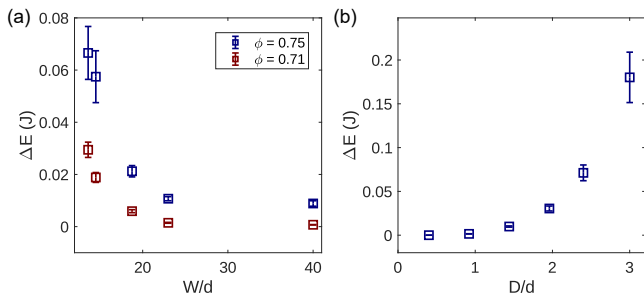
FIG. 2. $\langle \Delta E \rangle$ as a function of: (a) channel width W [at $\phi = 0.75$ and $D = 1.26 d_s$] and (b) intruder size D [at $\phi = 0.68$ and $W = 14 d_s$]. Here, d_s is the diameter of the small particles. In panel (a) we adjust κ and drive angular velocity so that the spring is pulled at the same tangential speed, fixing the linear rate of force increase when the intruder is stationary. Error bars correspond to the standard error of the mean.
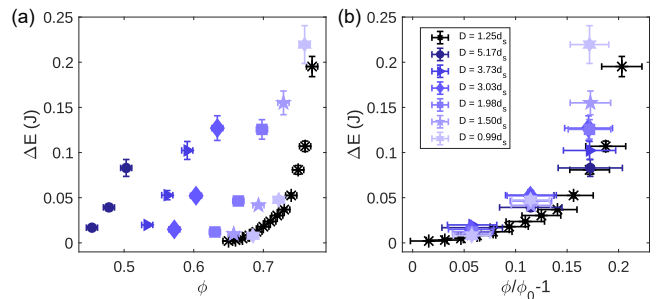

FIG. 3. (a) $\langle \Delta E \rangle$ as a function of ϕ for different intruder sizes. (b) Same as (a) as a function of the rescaled parameter $\phi/\phi_0 - 1$. The black symbols correspond to the experimental data from Fig. 1(c).

in a slip event. Other works, see in particular [23], have focused on this divergence in similar systems. Here we turn our attention to the onset of stick-slip behavior, which occurs at ϕ_0.

The transition at ϕ_0 has not been reported in other studies on intruders mainly because most of these studies are carried out in a 3D system under gravity [13, 18]. Under such conditions, the intruder's wake is constantly filled in. In cases where constant volume conditions in 2D were used and a wake developed, the focus was on packing fractions close to the jamming point rather than packing fractions at very low reaction forces [8, 17, 23], and often a steady state was never achieved. According to previous experiments, the extent of the wake becomes a sensitive parameter to identify different aspects of the dynamics (i.e., stick–slip versus full jamming) [23]. In a previous work [19] utilizing a similar Couette geometry, the granular sample was continuously stirred behind the intruder to remove its wake. For this stirred system, a crossover in the mean force as a function of ϕ (from linear to power-law with exponent 1.53) was observed at a similar packing fraction ϕ_0 to what we observe in our experiments [19]. For our non-stirred system this becomes a clearly identifiable transition.

As mentioned above, stick–slip dynamics develop for $\phi > \phi_0$, and $\langle \Delta E \rangle$ can be measured, increasing continuously with ϕ up to $\phi_c \approx 0.8$, where the system completely jams (see Fig. 1(c)). Beyond ϕ_c, the spring force increases until particles in experiments buckle out of plane, or, in simulations, numerical instabilities develop or the maximum run time is reached.

A remarkable feature in Fig. 1(c) is the collapse of the data obtained from the different interaction parameters and the grain number ratios. Note that no scaling has been applied to either the $\langle \Delta E \rangle$ or the ϕ axes. This universal response resembles the well-known behaviour of sheared granular materials at the limit of low inertial number I [24]. In this limit, the effective friction $\mu(I)$ and

the shear strength are insensitive to details of the grain–grain interactions [25] and the particle size distribution [26]. In our intruder scenario, however, the stick–slip behavior differs significantly from the dynamics observed in a simple shear experiment.

It is important to mention that ΔE is independent of basal friction for $\mu_{\mathrm{BF}} > 0.2$. For very low basal friction, particles set in motion behind the intruder after a slip tend to remain in motion, filling in the wake left by the intruder before coming to rest. This effect resembles the stirring mechanism implemented in [19]. This leads to a different dynamics over all, which we do not investigate further in present work.

We explore now the effect of geometric factors, including intruder and system size, on the intruder dynamics, which have been shown to affect the force fluctuations [23]. In Fig. 2(a) we show $\langle \Delta E \rangle$ obtained from simulations as a function of W with fixed ϕ ($\phi = 0.68$). A change in W implies a change in the radial position R of the intruder; the same torque spring and angular drive velocity would then lead to a different tangential stiffness and tangential velocity. To keep the effective linear stiffness of the spring and the effective tangential driving speed the same in all cases, we set the spring constant $\kappa = \kappa_0 (R/R_0)^2$ and the angular velocity of the driver $\omega = \omega_0 (R_0/R)$, where R_0 is the radial position for our experimental system size that we use as reference. We find that $\langle \Delta E \rangle$ decreases with increasing W, suggesting that stick–slip is a finite-size effect and may disappear for large system sizes. Similarly, in Fig. 2(b) we plot $\langle \Delta E \rangle$ as a function of the intruder diameter D at $\phi = 0.68$. Here $\langle \Delta E \rangle$ is zero for very small intruders and becomes finite at a minimum intruder size, then increases smoothly with D in agreement with [23] and [19].

The data collapse shown in Fig. 1(c) suggests that we plot $\langle \Delta E \rangle$ as a function of ϕ for different values of D and W. Figure 3(a) shows experimental data for seven choices of D. We note that the transition to zero force (when the open channel forms) occurs at a different value ϕ_0 for each D. The data collapse onto a single curve
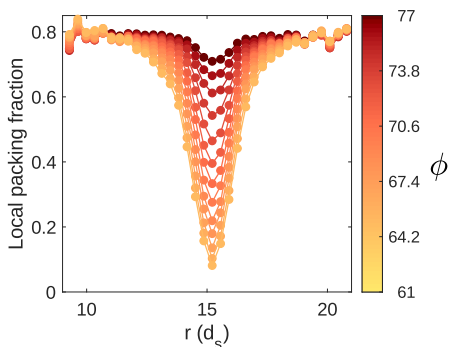
FIG. 4. Local packing fraction extracted from experiments with $D = 1.26d_s$ as a function of distance from the center of the Couette r and for different global packing fractions ϕ (see color scale), averaged over all steady state sticking periods.

when plotted against $\phi/\phi_0 - 1$, a measure of the relative distance to the transition, as shown in Fig. 3(b). The value of ϕ_0 for each D was estimated by lowering the packing fraction ϕ until no steady state dynamics were observed. Surprisingly, there is no need for any rescaling of the energies; furthermore, the data shown in Fig. 1(c) (see black symbols in Fig. 3(b)) also lie on the same curve.

The full data collapse we observe can be explained by a simple argument for the dependence of ϕ_0 on W and D. We assume that ϕ_0 corresponds to the highest ϕ (global packing fraction) at which the intruder is able to clear a channel that will allow it to move freely without contacting particles after a few revolutions. Therefore, ϕ_0 can be computed from the area of the Couette cell $A_{\text{Couette}} = \pi(R_{\text{out}}^2 - R_{\text{in}}^2)$, the area $A_{\text{free}} = \pi[(R_{\text{in}} + W/2 + D/2)^2 - (R_{\text{in}} + W/2 - D/2)^2]$ of the free channel necessary for the intruder to move freely, and the maximal packing fraction ϕ_{max} at which particles are packed into the two regions on each side of the intruder's path around the center of the annulus. We have

$$\phi_0 = \frac{\phi_{\text{max}}(A_{\text{Couette}} - A_{\text{free}})}{A_{\text{Couette}}} = \phi_{\text{max}}\frac{W - D}{W}. \quad (1)$$

We have measured ϕ_{max} in the experiments from average local ϕ profiles shown in Fig. 4, and the value is $\phi_{\text{max}} \approx 0.79$ at the boundaries. The local packing fraction as a function of radial position in the channel is computed using a sliding annular window of width $\sim 1.4d_s$. For a given annular window, the area occupied by particles is divided by the window's area for each sticking period configuration, and these results are then averaged. As expected, these local packing fraction profiles are not simple square wells; a clear boundary layer appears at each side of the intruder. To account for the boundary layer (which we assume to be roughly constant in width) we introduce a correction to Eq. (1) following a strategy similar to previous works [27, 28]. The corrected equation is
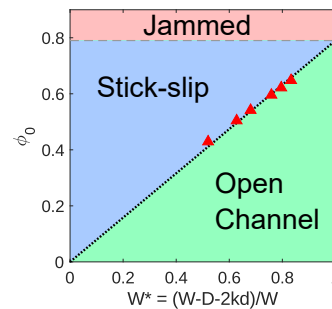

FIG. 5. ϕ_0 as a function of $(W - D - 2kd)/W$ with $k = 0.62$, obtained by linear regression. The black dotted line corresponds to Eq. (2) with $\phi_{\text{max}} = 0.79$, and the horizontal gray dashed line corresponds to ϕ_{max}.
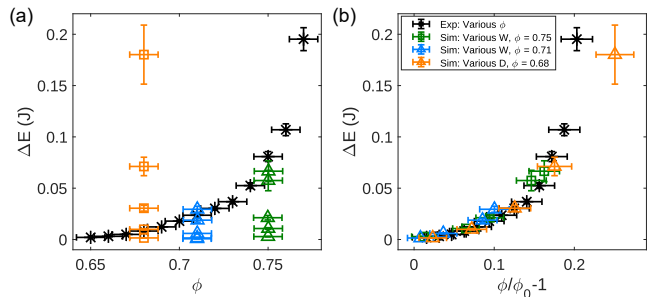

FIG. 6. (a) $\langle\Delta E\rangle$ as a function of ϕ for a range of configurations of the system that we tested with various D and W. (b) $\langle\Delta E\rangle$ as a function of $\phi/\phi_0 - 1$ for the data in panel (a). The actual value of ϕ_0 in each case has been estimated by using Eq. (2). The black symbols correspond to the experimental data from Fig. 1(c).

$$\phi_0 = \phi_{\text{max}}\frac{W - D - 2kd}{W}, \quad (2)$$

where k is a phenomenological parameter that measures the width of each of the two boundary layers in units of grain diameters. Figure 5 shows the values of ϕ_0 estimated from Fig. 3 as a function of $W^* = (W - D - 2kd)/W$. Having obtained the value k from experiments carried out using different intruder sizes D, we use Eq. (2) to compute ϕ_0 for all other cases of W and D considered in this work. As will be demonstrated below, statistical properties of the intruder's dynamics indeed collapse when plotted against $\phi/\phi_0 - 1$ with ϕ_0 computed in this manner.

Figure 6 shows $\langle\Delta E\rangle$ for simulations carried out with different D and W at fixed packing fractions. Figure 6(b) shows the data when plotted against $\phi/\phi_0 - 1$. The collapse suggests that one single parameter (ϕ_0) suffices to describe the stick–slip response of the granular system constrained at constant volume when an intruder attached to a spring is dragged at low speed. Again, these data also collapse with the data from the experiments and simulations shown in Figs. 1(c) and 3 (see

black symbols).

Figure 5 suggests a nontrivial prediction regarding the limit of infinitely large systems. If $W \gg D$ then $W^* \to 1$. In this limit, the value of ϕ_0 tends to 0.79. This means that no force will be exerted on the intruder for $\phi < 0.79$. As we mentioned above, when $\phi \gtrsim 0.8$ we observe a complete jamming of the system. Therefore, the actual range of packing fractions for which a stick-slip steady state can be established becomes very narrow for large systems, possibly vanishing in the large W limit. Of course, the $W^* \to 1$ limit has to be taken with caution. The time taken to complete a revolution and eventually reach the steady state diverges with the system size in this annular geometry.

Conclusions – We have described a new regime in the dynamics of an intruder dragged through a granular medium. In our experiments and simulations the system is confined to a fixed volume, and the granular material reaches a steady state after the intruder passes through a few revolutions. Due to the friction with the substrate, particles pushed aside tend to rest outside of the intruder's path in subsequent passes. At low packing fractions, the intruder is thus able to open a channel so that in the steady state no resistance is supplied by the medium. Above a critical packing fraction ϕ_0 a sharp transition occurs and the channel cannot be fully opened, which leads to a finite mean reaction force that increases with the global packing fraction ϕ.

We have found that ϕ_0 and $\langle \Delta E \rangle(\phi)$ are universal in the sense that over a broad parameter range they are independent of the details of the particle–particle interaction, particle–substrate interaction and particle size distribution. While they are very sensitive to the system size and the intruder size, $\langle \Delta E \rangle(\phi)$ can be collapsed onto a single master curve if plotted against $\phi/\phi_0 - 1$. We have proposed a simple model for the dependence of ϕ_0 on W and D that is in excellent agreement with the data. While we have studied this model with one particular driving spring constant, the collapse of statistics related to stick-slip is picted to be robust, even though the time and energy scales of stick-slip will change when the driving spring changes. Future works may explore whether the collapse we explain is robust in other contexts, for example, when the spring is infinitely stiff and the intruder is driven at a constant velocity. Further work is also needed in the direction of analysis of force networks, in particular in light of friction independence of our results for the energy drop (for sufficiently large friction). Some preliminary work in this direction can be found in [29, 30]. We lastly note that our results may have implications for 3D systems, as demonstrated in recent experiments [31] where the drag force on a submerged intruder reaches a steady state after the intruder retraces its path in a 3D granular material. Our findings may also find particular utility in the context of testing various novel theoretical approaches for dense granular media such as

non-local rheology models [32, 33].

―――――――

* luis.pugnaloni@exactas.unlpam.edu.ar
[1] G. Sanglerat, *The penetrometer and soil exploration* (Elsevier, 2012).
[2] J. Geng, D. Howell, E. Longhi, R. P. Behringer, G. Reydellet, L. Vanel, E. Clément, and S. Luding, Phys. Rev. Lett. **87**, 035506 (2001).
[3] J. Geng and R. P. Behringer, Phys. Rev. Lett. **93**, 238002 (2004).
[4] I. Goldhirsch and C. Goldenberg, Eur. Phys. J. E **9**, 245 (2002).
[5] A. P. F. Atman, P. Brunet, J. Geng, G. Reydellet, G. Combe, P. Claudin, R. P. Behringer, and E. Clément, J. Phys.: Condens. Matter **17**, S2391 (2005).
[6] B. P. Tighe and J. E. S. Socolar, Phys. Rev. E **77**, 031303 (2008).
[7] A. Seguin, C. Coulais, F. Martinez, Y. Bertho, and P. Gondret, Phys. Rev. E **93**, 012904 (2016).
[8] R. Candelier and O. Dauchot, Phys. Rev. Lett. **103**, 128001 (2009).
[9] A. Fiege, M. Grob, and A. Zippelius, Granular Matter **14**, 247 (2012).
[10] T. Faug, Eur. Phys. J. E **38**, 1 (2015).
[11] S. Kumar, K. A. Reddy, S. Takada, and H. Hayakawa, arXiv preprint arXiv:1712.09057 (2017).
[12] S. Takada and H. Hayakawa, Granular Matter **22**, 1 (2020).
[13] J. Hilton and A. Tordesillas, Phys. Rev. E **88**, 062203 (2013).
[14] A. Tordesillas, J. E. Hilton, and S. T. Tobin, Phys. Rev. E **89**, 042207 (2014).
[15] C. M. Carlevaro, R. Kozlowski, L. A. Pugnaloni, H. Zheng, J. E. S. Socolar, and L. Kondic, Phys. Rev. E **101**, 012909 (2020).
[16] R. Candelier and O. Dauchot, Phys. Rev. E **81**, 011304 (2010).
[17] C. J. Olson Reichhardt and C. Reichhardt, Phys. Rev. E **82**, 051306 (2010).
[18] I. Albert, P. Tegzes, R. Albert, J. G. Sample, A. L. Barabási, T. Vicsek, B. Kahng, and P. Schiffer, Phys. Rev. E **64**, 031307 (2001).
[19] J. Geng and R. P. Behringer, Phys. Rev. E **71**, 011302 (2005).
[20] R. Kozlowski, C. M. Carlevaro, K. E. Daniels, L. Kondic, L. A. Pugnaloni, J. E. S. Socolar, H. Zheng, and R. P. Behringer, Phys. Rev. E **100**, 032905 (2019).
[21] E. Catto, "Iterative dynamics with temporal coherence," (2005), available at https://box2d.org/downloads/.
[22] See Supplemental Material at [URL will be inserted by publisher] for sample raw signals form the force sensor

and additional plots showing the collapse of other stick–slip dynamic descriptors plotted against $\phi/\phi_0 - 1$.

[23] E. Kolb, P. Cixous, N. Gaudouen, and T. Darnige, Phys. Rev. E **87**, 032207 (2013).

[24] G. MiDi, Eur. Phys. J. E **14**, 341 (2004).

[25] F. da Cruz, S. Emam, M. Prochnow, J.-N. Roux, and F. m. c. Chevoir, Phys. Rev. E **72**, 021309 (2005).

[26] D. Cantor, E. Azéma, P. Sornay, and F. Radjai, Phys. Rev. E **98**, 052910 (2018).

[27] K. W. Desmond and E. R. Weeks, Phys. Rev. E **80**, 051305 (2009).

[28] W. A. Beverloo, H. A. Leniger, and J. Van de Velde, Chem. Eng. Sci. **15**, 260 (1961).

[29] R. Kozlowski, H. Zheng, K. E. Daniels, and J. E. S. Socolar, EPJ Web of Conferences **249**, 06010 (2021).

[30] R. Kozlowski, H. Zheng, K. E. Daniels, and J. E. S. Socolar, Soft Matter **17**, 10120 (2021).

[31] F. Guillard, Y. Forterre, and O. Pouliquen, Phys. Rev. Lett. **110**, 138303 (2013).

[32] O. Pouliquen and Y. Forterre, Phil. Trans. Royal Soc. A: Math., Phys. Eng. Sci. **367**, 5091 (2009).

[33] K. Kamrin and G. Koval, Phys. Rev. Lett. **108**, 178301 (2012).